Electronic Structures of Dinitrogen Tetroxide and Diboron Tetrafluoride and an Analysis of Their Conformational Stabilities

James M. Howell* and John R. Van Wazer

Contribution from the Department of Chemistry, Brooklyn College, City University of New York, Brooklyn, New York 11210, and the Department of Chemistry, Vanderbilt University, Nashville, Tennessee 37235. *Received April 23, 1974*

Abstract: The electronic wave functions of N_2O_4 and B_2F_4 were determined in moderately sized *ab initio* computations. The rotational barriers of both molecules were calculated and analyzed in terms of lone-pair interactions between nonadjacent oxygen or fluorine atoms, along with lone-pair donation into the central σ^* bond. Previously suggested alternative electronic configurations, where the NO_2 units are bonded only by π interactions, were considered for the ground state of N_2O_4 but were found to be dissociative and thus of little importance.

Although the two A_2Y_4 molecules dinitrogen tetroxide, N_2O_4, and diboron tetrafluoride, B_2F_4, are isoelectronic, each having 34 valence-shell electrons, they may have different equilibrium gas-phase geometries. In the gas phase, N_2O_4 exhibits the planar, D_{2h}, structure[1] with eclipsed oxygens, **1**, but the conformation of B_2F_4 is more uncertain. Early studies[2a] indicate either the staggered, D_{2d}, conformation, **2**, or free rotation, while a more recent investigation favors the planar form,[2b] **1**. A 1957 study by Snyder and Hisatsune[3] yielded a rotational barrier of 2.9 kcal/mol for N_2O_4. The energy barrier to rotation for B_2F_4 is presumably rather small, since in addition to the D_{2d} *vs.* D_{2h} uncertainty for the gas phase a crystal structure determination[4] favors a planar conformation. The rotational barrier of B_2Cl_4, which is normally staggered, has been determined by Hedberg[5] to be about 1.85 kcal/mol.

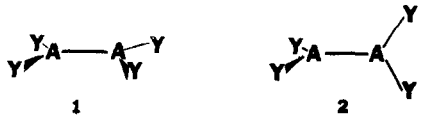

1 **2**

In this paper, we report some *ab initio* calculations on the electronic structure of both N_2O_4 and B_2F_4 and present a rationale for the gas-phase rotational barriers of the two compounds.

A fundamental matter to the study of N_2O_4 is its electronic configuration. Coulson[6] proposed some time ago that both the σ and σ^* N–N levels might be occupied, with the net bonding between the two NO_2 units being provided by a "π-type" interaction, a "π-only" bond. This suggestion was an ingenious attempt to explain several of the observed geometric parameters of the N_2O_4 molecule (*i.e.* the N–N bond length of 1.75–1.78 Å being substantially longer than the N–N distance of 1.47 Å in hydrazine, H_2N–NH_2; the preference for the eclipsed D_{2h} structure; and the relatively high rotational barrier).

The possibility of alternative electronic structures has been investigated semiempirically in an indirect fashion by Brown and Harcourt[7] and by Serre and LeGoff.[8] We now attack the problem by determining the total energy of the various single-determinant electronic configurations as a function of the N–N bond length.

There have been many semiempirical investigations of the electronic structure of N_2O_4[7,9,10] and B_2F_4.[10,11] An *ab initio* investigation of N_2O_4 and B_2F_4 has appeared reporting a higher energy.[12] Although interpretations of the rotational barrier have been centered on π interactions[13] of the AY_2 units, the present study is found naturally to focus on the interaction of the axial lone pairs, those which are more or less parallel to the A–A axis. The analysis that will be presented draws on the work of Stohrer and Hoffmann[14] on strained tricyclic hydrocarbons and by Epiotis[15] on 1,4-nonbonded attractive interactions in halogenated hydrocarbons.

Calculational Details[16]

The *ab initio* calculations were carried out with the programs POLYATOM and IBMOL V using two different sizes of atom-optimized Gaussian basis sets. The smaller set, which consisted of five s-type and two sets of p-type exponents for each atom, *i.e.* the (52/52) set,[17] was used to carry out limited geometry optimizations. The larger basis set[18] consisted of seven s-type and three sets of p-type exponents for each atom (73/73), and this was employed for the final calculations on which were based the energies and population analyses presented in the tables. For the staggered conformations, the molecular orbitals of e symmetry were established so that each member of a degenerate pair would be symmetric to reflection in the plane defined by one of the AY_2 groups and antisymmetric to reflection in the plane of the other.

Extended Hückel calculations[19] were also performed to aid in the analysis of the interactions in the molecules. The parameters of Hoffmann[20] along with the *ab initio* optimized geometries were employed. The results of the extended Hückel method were roughly similar to those of the *ab initio* studies. This extended Hückel program provided the opportunity to delete interactions between certain specific atomic orbitals by simply setting the off-diagonal pseudo-Fock matrix element, H_{ij}, along with the corresponding overlap matrix element, S_{ij}, for the pertinent interaction to zero. There is a fundamental difference between the extended Hückel method and the SCF *ab initio* method. The sum of the molecular orbital energies equals the total energy for the Hückel method but not the *ab initio*.

Results and Discussion

Overall Results. In the limited geometry optimization for N_2O_4, the energy was minimized only with respect to the N–N bond length with a preliminary optimization in the (52/52) basis set followed by another in the neighborhood of the (52/52) minimum using the (73/73) basis set. The final optimized value for the N–N distance was 1.67 Å, while the N–O bond length of 1.18 Å and the ONO angle of 133.7° were taken from Smith and Hedberg.[1a] It is interesting that the optimized N–N bond distance increases by

Table I. Summary of Calculated Quantities for N_2O_4 and B_2F_4 Using (73/73) Gaussian Basis Sets

	N_2O_4		B_2F_4	
	Planar (D_{2h})	Staggered (D_{2d})	Planar (D_{2h})	Staggered (D_{2d})
Total energy, au	−407.3650	−407.3465	−446.7441	−446.7446
Nuclear repulsion, au	242.8180	241.6254	203.1890	202.5764
Mulliken population, e				
Gross atomic charges				
N/B	+0.519	+0.555	+0.696	+0.701
O/F	−0.260	−0.278	−0.348	−0.350
Overlap population				
N–N/B–B	0.231	0.307	0.063	0.075
N–O/B–F	0.441	0.451	0.723	0.724
$(O\cdots O)_{1,3}/(F\cdots F)_{1,3}$[a]	−0.144	−0.146	−0.060	−0.059
$(N\cdots O)_{1,3}/(B\cdots F)_{1,3}$	−0.130	−0.118	−0.080	−0.081
$(O\cdots O)_{1,4}/(F\cdots F)_{1,4}$	0.033	0.006	0.000	0.000

[a] The subscripts indicate the separation of the atoms involved. Thus for N_2O_4, $(O\cdots O)_{1,3}$ represents the overlap of the gem oxygens; $(N\cdots O)_{1,3}$, the overlap between a nitrogen and an oxygen bonded to its neighboring nitrogen; and $(O\cdots O)_{1,4}$, the overlap between the oxygen on one nitrogen with an oxygen (cis in the D_{2h} case) on the other.

about 0.02 Å in shifting from the (52/52) to the (73/73) basis set. Employing a still larger basis set would probably decrease but perhaps not eliminate the gap between the optimized bond length and the experimental value of 1.75 or 1.782 Å.[1] An additional factor causing the optimized N–N bond length to be 5% shorter than the experimental value might be configuration-interaction mixing of doubly excited configurations having two electrons in an N–N σ^* orbital[9e] into the ground state. Because of the delicate balancing of factors in the B_2F_4 electronic structure, the geometry of this molecule was optimized in the (52/52) set with respect to both the B–B bond length and the FBF angle (optimized values 1.72 Å and 110°), while the B–F bond distance was held constant at the experimental value[2a] of 1.32 Å.

Some overall results from these calculations are presented in Tables I and II for the optimized molecular geometries. From the data of Table I, we see that the rotational barrier calculated for N_2O_4 is 11.6 kcal/mol for the (73/73) basis set and 0.3 kcal/mol for B_2F_4 in the same basis set. The barriers obtained in the smaller (52/52) calculation were 10.7 and 0.1 kcal/mol, respectively. Note that the calculations agree with experiment in assigning the planar conformation to the N_2O_4 molecule. The calculated rotational barrier of B_2F_4 favors the D_{2d} conformer by 0.3 kcal/mol, in conflict with the more recent experimental work.[2b] The analysis that follows below concentrates on a comparison of rotational barriers of the two molecules: N_2O_4 definitely favoring the planar, D_{2h} form, while B_2F_4 has only a very small barrier to rotation. From parabolic fitting of the bottom regions of the curves giving the variation of the calculated total energy with internuclear distance, we have theoretically estimated the force constant for stretching of the N–N bond in N_2O_4 to be 3.8 mdyn/Å and of the B–B bond in B_2F_4 to be 3.0 mdyn/Å. The observed value[21] for N_2O_4 is 1.47 mdyn/Å and, by way of comparison, for ethylene,[22] 9.47 mdyn/Å.

Description of the Electronic Structure.[16] N_2O_4 and B_2F_4 are isoelectronic molecules, each having 17 filled valence-shell molecular orbitals. As expected, when both of the molecules are in the same geometry, there is a marked similarity between their molecular orbitals. This similarity is shown by the data of Tables III *vs.* V and IV *vs.* VI. For the planar conformers, the molecular orbitals of these A_2Y_4 molecules are readily classifiable according to their dominant contributions to the A–A bonding and to the A–Y bonding, either σ or π with respect to the designated bond axis. In addition, the molecular orbitals which are dominated by the lone-pair character of the Y atoms may also be so characterized with respect to the A–Y axis involved or the molecular axis on which the A–A bond lies. Such characterizations based on Mulliken population analyses by atomic-orbital symmetry and on electron-density plots are given for the filled valence-shell molecular orbitals of the planar conformation of N_2O_4 in Table III and of B_2F_4 in Table V.

Table II. Analysis of the Mulliken Population for N_2O_4 and B_2F_4 in which the Molecular Orbitals Have Been Classified According to Nodal Characteristics with Respect to the N–N or B–B Bond Axis

		N_2O_4		B_2F_4	
		Planar D_{2h}	Staggered D_{2d}	Planar D_{2h}	Staggered D_{2d}
		Gross Atomic Populations			
A	σ	4.397	4.373	3.583	3.580
	π	1.100	1.101	0.299	0.311
	π'	0.984	0.970	0.422	0.408
	$\pi + \pi'$	2.082	2.071	0.721	0.719
Y	σ	4.302	4.312	3.709	3.713
	π	1.450	1.453	1.851	1.854
	π'	2.509	2.512	2.789	2.787
	δ	1.000	1.000	1.000	1.000
	$\pi + \pi'$	3.959	3.965	4.640	4.640
		Overlap Populations			
A-Y	σ	0.102	0.102	0.336	0.335
	π	0.250	0.250	−0.151	0.151
	π'	0.089	0.098	0.236	0.237
	$\pi + \pi'$	0.339	0.348	0.387	0.388
A–A	σ	0.277	0.335	0.078	0.112
	π	−0.005		−0.029	
	π'	−0.044		0.014	
	$\pi + \pi'$	−0.048	−0.028	−0.014	−0.037
$(Y\cdots Y)_{1,4}$	σ	0.033	0.005	0.000	0.000
	π	0.000		0.000	
	π'	0.001		0.000	
	$\pi + \pi'$	0.001	0.000	0.000	0.000

In discussing A–A bonding, it should be noted that, with respect to this bond axis in the planar molecule, molecular orbitals which are σ exhibit a_g and those which are σ^* exhibit b_{1u} symmetry. Population analyses and electron-density plots indicate that the a_g and b_{1u} orbitals of the planar form may be considered to transform into the a_1 and b_2 orbitals respectively, of the staggred form. The usual "π" orbitals for A_2Y_4 planar molecules must be antisymmetric to reflection in the molecular plane. Thus, the π orbitals, with respect to the A–A bond, exhibit b_{3u} and the π^* orbitals show b_{2g} symmetry, with the equivalent orbitals in the staggered conformation having e symmetry. The set of orbitals at right angles, in which the A–A axis lies in a nodal plane perpendicular to the molecular plane, may be designated for the planar molecule as π' having b_{2u} symmetry

Table III. Mulliken Population Analysis of the Valence Molecular Orbitals of Planar N_2O_4 Calculated in a (73/73) Basis Set

N_2O_4, Orbital	D_{2h} Energy	Gross atomic population N	Gross atomic population O	Overlap populations N–N	Overlap populations N–O	Overlap populations $(O\cdots O)_{bi}$	Dominant character[a] N–N bond	Dominant character[a] N–O bond	Dominant character[a] Lone pair
$6a_g$	−0.466	0.195	0.403	0.320	−0.188	0.045	$(\vec{p}_\sigma-\overleftarrow{p}_\sigma)$	$(p_\pi'-p_\pi')^*$	p_π'
$1a_u$	−0.503	0.0	0.500	0.0	0.0	−0.005			p_π
$1b_{1g}$	−0.517	0.0	0.500	0.0	0.0	0.005			p_π
$4b_{3g}$	−0.533	0.011	0.495	−0.011	0.003	−0.019			p_π'
$4b_{2u}$	−0.588	0.028	0.486	0.005	0.007	0.018			p_π'
$5b_{1u}$	−0.696	0.287	0.357	−0.455	0.161	−0.020	$(\vec{p}_\sigma-\overleftarrow{p}_\sigma)^*$	$(p_\pi'-\vec{p}_\pi')$	p_π'
$3b_{3g}$	−0.767	0.203	0.399	−0.078	−0.120	−0.001	$(p_\pi'-p_\pi')^*$	$(p_\sigma-sp_\sigma)$	sp_σ
$1b_{2g}$	−0.771	0.507	0.247	−0.099	0.135	−0.001	$(p_\pi-p_\pi)^*$	$(p_\pi-\vec{p}_\pi)$	
$3b_{2u}$	−0.790	0.208	0.396	0.048	−0.081	0.001	$(p_\pi'-p_\pi')$	$(p_\sigma-sp_\sigma)$	sp_σ
$1b_{3u}$	−0.835	0.593	0.204	0.095	0.116	0.001	$(p_\pi-p_\pi)$	$(p_\pi-\vec{p}_\pi)$	
$5a_g$	−0.870	0.264	0.368	−0.001	−0.049	0.013	$(sp_\sigma-\vec{sp}_\sigma)^*$	$(p_\sigma-\vec{sp}_\sigma)^*$	sp_σ
$4b_{1u}$	−0.895	0.189	0.405	−0.064	−0.121	−0.005	$(\overleftarrow{s}_\sigma-\vec{s}_\sigma)$	$(s_\sigma-\vec{s}_\sigma)^*$	s_σ
$4a_g$	−1.078	0.656	0.172	0.444	−0.035	0.001	$(sp_\sigma-sp_\sigma)$	$(s_\sigma-s_\sigma)^*$ $(p_\pi'-\overleftarrow{p}_\pi')$	
$2b_{3g}$	−1.527	0.276	0.362	−0.018	0.150	−0.005	$(p_\pi'-p_\pi')^*$	$(p_\sigma-\overleftarrow{s}_\sigma)$	
$2b_{2u}$	−1.552	0.257	0.372	0.010	0.128	0.007	$(p_\pi'-\vec{p}_\pi')$	$(\vec{p}_\sigma-\overleftarrow{s}_\sigma)$	
$3b_{1u}$	−1.717	0.370	0.315	−0.014	0.171	−0.005	$(\overleftarrow{s}_\sigma-\vec{s}_\sigma)^*$	$(\vec{s}_\sigma-\overleftarrow{s}_\sigma)$	
$3a_g$	−1.766	0.436	0.282	0.049	0.161	0.004	$(\overleftarrow{s}_\sigma-\vec{s}_\sigma)$	$(\vec{s}_\sigma-\overleftarrow{s}_\sigma)$	

[a] In this A_2Y_4 molecule, the dominant character of each bond is presented with respect to its own axis and of each Y-atom lone pair with respect to the A–Y bond axis. The symbols are employed as follows: () for bonding ()* for antibonding; with s or p standing for the contributing atomic orbital and sp for this contributing hybrid. The π, σ, π' character of the bond is indicated by the subscripts and the direction of the superscript arrows indicates polarization along the reference bond axis of the contributing atomic orbitals, with the greater electron density being on the side of the arrowhead.

Table IV. Mulliken Population Analysis of the Valence Molecular Orbitals of Staggered N_2O_4 Calculated in a (73/73) Basis Set

N_2O_4, Orbital	D_{2d} Energy	Gross atomic populations N	Gross atomic populations O	Overlap populations N–N	Overlap populations N–O	Overlap populations $(O\cdots O)_{bi}$
$6a_1$	−0.451	0.186	0.407	0.302	−0.178	0.009
$1a_2$	−0.505	0.0	0.500	0.0	0.0	−0.002
$1b_1$	−0.513	0.0	0.500	0.0	0.0	0.002
5e	−0.566	0.039	0.980	−0.005	0.011	−0.001
$5b_2$	−0.711	0.266	0.367	−0.370	0.154	−0.004
4e	−0.771	0.529	0.735	−0.130	−0.087	0.000
3e	−0.815	0.981	0.510	0.106	0.152	0.000
$5a_1$	−0.864	0.265	0.367	0.002	−0.038	0.001
$4b_2$	−0.902	0.193	0.403	−0.072	−0.141	−0.001
$4a_1$	−1.082	0.657	0.172	0.441	−0.029	0.000
2e	−1.543	0.520	0.740	0.001	0.270	0.000
$3b_2$	−1.721	0.372	0.314	−0.016	0.171	−0.001
$3a_1$	−1.768	0.433	0.283	0.049	0.161	0.001

and $(\pi')^*$ having b_{3g} symmetry. Again, upon rotation to the staggered conformation, these two orbitals convert into an e pair. Note that the two molecular orbitals $1b_{1g}$ for the planar conformer (or $1b_1$ for the staggered) and $1a_u$ (or $1a_2$) appearing among the valence orbitals of each molecule exhibit no A–A or A–Y overlap population but only lone-pair character, since with respect to the A–A bond axis these orbitals would be δ and δ^*, respectively. With no d character allowed to the A atoms in the calculations, these orbitals cannot include bonding character and, even if atomic d orbitals had been incorporated into the basis set, we would have expected negligible A–A overlap in these orbitals for the N_2O_4 and B_2F_4 molecules.

According to this analysis of the molecular orbitals in terms of A–A bond character, the *ab initio* calculations give the following ordering (from more to less stability) of the valence orbitals of N_2O_4, shown in Tables III and IV: 3σ, $3\sigma^*$, $2\pi'$, $2(\pi')^*$, 4σ, $4\sigma^*$, 5σ, 1π, $3\pi'$, $1\pi^*$, $3(\pi')^*$, $5\sigma^*$, $4\pi'$, $4(\pi')^*$, 1δ, $1\delta^*$, and 6σ. For B_2F_4 (see Tables V and VI), the calculated ordering is: 3σ, $3\sigma^*$, $2\pi'$, $2(\pi')^*$, 4σ, $4\sigma^*$, 5σ, $3\pi'$, $3(\pi')^*$, 1π, $1\pi^*$, $5\sigma^*$, 1δ, $1\delta^*$, $4\pi'$, $4(\pi')^*$, and 6σ. Although there is some difference between the two molecules in this ordering with respect to orbital energy, it is important to note that, according to the *ab initio* results, there is an antibonding orbital for each bonding orbital in all cases except for the outermost orbital 6σ. Since the N–N overlap population for this orbital is larger in the case of the planar as compared to the staggered form of N_2O_4 (see Tables III and IV) and the B–B overlap of this orbital is about the same for the two conformers (see Tables V and VI), we might set up a crude rationale for the observed conformational stability on this basis. However, as indicated by the population data of Table II, the matter is more complex than this and hence must be argued in a more subtle fashion.

Electronic Configuration of N_2O_4. Alternative ground-state electronic configurations of N_2O_4 have been proposed[6] wherein a pair of electrons is removed from a high-lying lone-pair molcular orbital (say, either the $1a_u$ or $1b_{1g}$ orbital) and placed in the N–N σ^* molecular orbital, $6b_{1u}$. The electronic configuration which turns out to have the lowest energy may be specified for the planar molecule as $\ldots (4b_{3g})^2(1b_{1g})^2(1a_u)^2(6a_g)^2$, referred to as Σ; and it is the configuration corresponding to Tables I through VII. Alternative configurations are $\ldots (4b_{3g})^2(1a_u)^2(6a_g)^2(6b_{1u})^2$, referred[23] to as $\Pi 1$ and $\ldots (4b_{3g})(1b_{1g})^2(6a_g)^2(6b_{1u})^2$, referred to as $\Pi 2$. In both the $\Pi 1$ and $\Pi 2$ cases, the N–N σ bonding present in the $6a_g$ orbital has been counterbalanced through occupation of the N–N σ^* orbital, $6b_{1u}$.

We have attempted to test this interesting suggestion by determining the potential curve of each configuration for a motion whereby the two NO_2 units are moved apart from each other. The results are shown in Figure 1, where it is obvious that the Σ configuration possesses a minimum near the experimentally determined N–N distance. However, the $\Pi 1$ and $\Pi 2$ configurations are not only less stable but, equally significant, possess no minimum out to an N–N distance of 4 Å; *i.e.*, they are probably dissociative. Similar operations may be carried out by promoting the pair of electrons from either the $3b_{2u}$ or $3b_{3g}$ orbitals to the $6b_{1u}$ orbital to give a $\Pi'1$ or $\Pi'2$ configuration, as well as by pro-

Table V. Mulliken Population Analysis of the Valence Molecular Orbitals of Planar B_2F_4 Calculated in a (73/73) Basis Set

B_2F_4, Orbital	D_{2h} Energy	Gross atomic population B	Gross atomic population F	Overlap populations B–B	Overlap populations B–F	Overlap populations $(F\cdots F)_{cis}$	Dominant character[a] B–B bond	Dominant character[a] B–F bond	Dominant character[a] Lone pair
$6a_g$	−0.5354	0.556	0.222	0.505	−0.094	0.000	$(\vec{p}_\sigma-\overleftarrow{p}_\sigma)$	$(p_\pi'-p_\pi')^*$	
$4b_{3g}$	−0.6350	0.016	0.492	−0.013	0.016	0.000			p_π'
$4b_{2u}$	−0.6416	0.033	0.484	0.008	0.016	0.000			p_π'
$1a_u$	−0.6477	0.0	0.500	0.0	0.0	0.000			p_π
$1b_{1g}$	−0.6477	0.0	0.500	0.0	0.0	0.000			p_π
$5b_{1u}$	−0.7028	0.081	0.460	−0.771	0.128	0.000	$(\vec{p}_\sigma-\overleftarrow{p}_\sigma)^*$	$(p_\pi'-p_\pi')$	p_π'
$1b_{2g}$	−0.7114	0.136	0.432	−0.068	0.084	0.000	$(p_\pi-p_\pi)^*$	$(p_\pi-p_\pi)$	
$1b_{3u}$	−0.7225	0.163	0.419	0.039	0.067	0.000	$(p_\pi-p_\pi)$	$(p_\pi-\vec{p}_\pi)$	
$3b_{3g}$	−0.7390	0.124	0.438	0.001	0.072	0.000	$(p_\pi'-p_\pi')^*$[b]	$(p_\sigma-\vec{sp}_\sigma)$	sp_σ
$3b_{2u}$	−0.7565	0.157	0.422	0.018	0.060	0.000	$(\vec{p}_\pi'-\overleftarrow{p}_\pi')$	$(p_\sigma-\vec{p}_\sigma)$	p_σ
$5a_g$	−0.7738	0.299	0.350	0.155	0.063	0.000	$(\overleftarrow{sp}_\sigma-\vec{sp}_\sigma)$	$(p_\pi'-\vec{p}_\pi')$	p_π'
$4b_{1u}$	−0.8179	0.158	0.421	0.009	0.068	0.000	$(\overleftarrow{sp}_\sigma-\vec{sp}_\sigma)^*$	$(p_\sigma-\vec{sp}_\sigma)$	sp_σ
$4a_g$	−0.8406	0.329	0.336	0.166	0.058	0.000	$(\vec{sp}_\sigma-\overleftarrow{sp}_\sigma)$	$(\overleftarrow{p}_\sigma-\vec{sp}_\sigma)$	sp_σ
$2b_{3g}$	−1.6368	0.042	0.479	−0.001	0.034	0.000			s_σ
$2b_{2u}$	−1.6393	0.049	0.475	0.001	0.038	0.000			s_σ
$3b_{1u}$	−1.1824	0.077	0.461	0.002	0.055	0.000			s_σ
$3a_g$	−1.6848	0.081	0.459	0.002	0.058	0.000			s_σ

[a] In this A_2Y_4 molecule, the dominant character of each bond is presented with respect to its own axis and of each Y-atom lone pair with respect to the A–Y bond axis. The symbols are employed as follows: () for bonding and ()* for antibonding; with s or p standing for the contributing atomic orbital and sp for this contributing hybrid. The π, σ, π' character of the bond is indicated by the subscripts and the direction of the superscript arrows indicates polarization along the reference bond axis of the contributing atomic orbitals, with the greater electron density being on the side of the arrowhead. [b] There is a substantial admixture of boron 3p character resulting in a gerade π^* orbital contribution, which is B–B bonding according to the Mulliken overlap population.

Table VI. Mulliken Population Analysis of the Valence Molecular Orbitals of Staggered B_2F_4 Calculated in a (73/73) Basis Set

B_2F_4, Orbital	D_{2d} Energy	Gross atomic populations B	Gross atomic populations F	Overlap populations B–B	Overlap populations B–F	Overlap populations $(F\cdots F)_{1,4}$
$6a_1$	−0.535	0.554	0.223	0.501	−0.092	0.000
5e	−0.640	0.051	0.974	−0.008	0.033	0.000
$1a_2$	−0.650	0.0	0.500	0.0	0.0	0.000
$1b_1$	−0.650	0.0	0.500	0.0	0.0	0.000
$5b_2$	−0.705	0.080	0.460	−0.734	0.126	0.000
4e	−0.716	0.272	0.864	−0.058	0.145	0.000
3e	−0.751	0.303	0.849	0.029	0.137	0.000
$5a_1$	−0.775	0.302	0.349	0.158	0.063	0.000
$4b_2$	−0.819	0.158	0.421	0.009	0.068	0.000
$4a_1$	−0.842	0.328	0.336	0.165	0.058	0.000
2e	−1.639	0.092	0.954	0.000	0.074	0.000
$3b_2$	−1.684	0.077	0.462	0.002	0.054	0.000
$3a_1$	−1.686	0.081	0.459	0.002	0.058	0.000

moting these electrons from either orbital $1b_{3u}$ or $1b_{2g}$ to $6b_{1u}$ to give a Π3 or Π4 configuration. The potential curves of these four resulting configurations are similarly probably dissociative. Consequently, we conclude that the ground state is best described by the Σ configuration. Brown and Harcourt[7] and Serre and LeGoff[8] came to the same conclusion on the grounds that the Π1 and Π2 configurations were nearly degenerate and a linear combination of them would yield a triplet ground state which is not observed.

Reasons for suggesting the possibility of the Π and Π′ configurations included the preference of N_2O_4 for the planar geometry and the long N–N bond. In the following two sections of this paper, we have attributed the calculated planarity of the Σ configuration to the increased donation of the lone pairs into the N–N σ^* bond and the increased bonding of the 1,4 interaction that occurs in that geometry. The long N–N bond may also be associated with the lone-pair donation into the N–N σ^* orbital, an idea which has been advanced before by Brown and Harcourt.[7a,9d]

Conformer Stabilization by σ Orbitals. As shown in Table II, the charge shifts on conformer change of the A atoms occur mainly in the σ instead of the π or π' orbitals (as denoted with respect to the A–A bonds) for the N_2O_4 molecule; while for the B_2F_4 molecule, the moderately large charge shifts in the π and π' orbitals effectively cancel so that there is little change in either the σ or total π manifold. For the A–A overlap the largest change is in the σ instead of the π and π' orbitals for both N_2O_4 and B_2F_4.

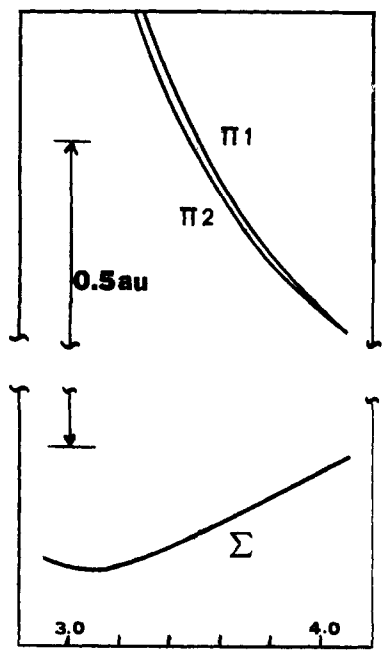

Figure 1. Potential-energy curves for three electronic configurations of N_2O_4. The horizontal axis refers to the N–N distance in Å. The two NO_2 units were held in the planar geometry, as is determined by electron diffraction.

In order to fully understand what is going on in the N_2O_4 molecule (as well as in B_2F_4), our detailed analysis will be couched in terms of symmetry-adapted molecular-orbital fragments. In Figure 2, the interaction and mixing occurring between the N–N σ and σ^* bonds of N_2O_4 and two symmetry-adapted combinations of the oxygen lone pairs lying in the plane of each AY_2 fragment and approximately parallel to the A–A bond axis are depicted for the planar

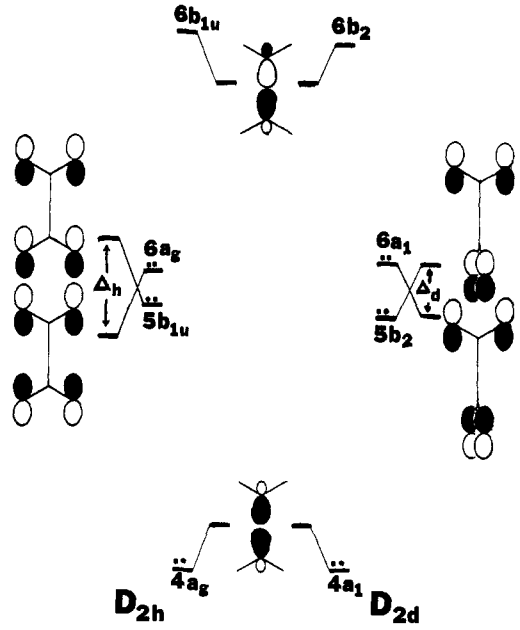

Figure 2. An interaction diagram for the σ-like orbitals of N_2O_4. In the center are the σ and σ^* N–N bonds. On the left-hand side are the symmetry-adapted combinations of the axial lone pairs in the planar, D_{2h}, molecular geometry while on the right appear the symmetry-adapted combinations of the axial lone pairs in the staggered, D_{2d}, geometry. The situation of B_2F_4 is similar except that the lone pairs would appear at substantially lower relative energies.

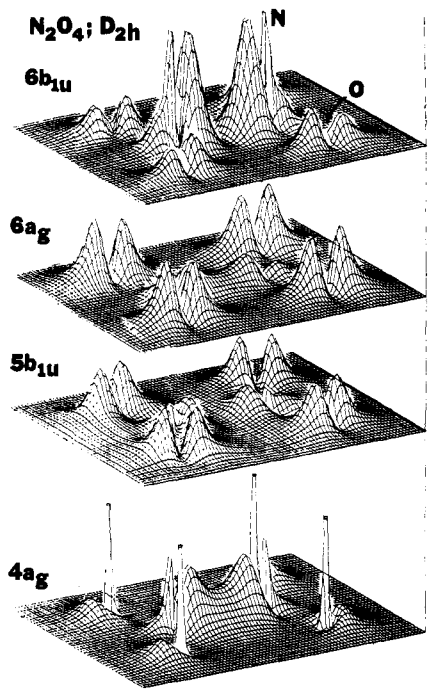

Figure 3. Computer-generated electron density plots for the $4a_g$ (dominant character N–N σ bonding), $5b_{1u}$ (antibonding O lone pair), $6a_g$ (bonding O lone pair), and the virtual $6b_{1u}$ (N–N σ^*) molecular orbitals evaluated in the molecular plane. Note the bonding incorporation of the N–N σ^* function into $5b_{1u}$ and antibonding mixing of the N–N σ orbital into $6a_g$.

and staggered geometries, using from the class of filled valence-shell orbitals only those molecular orbitals exhibiting large N–N overlap (see Tables III and IV). This figure illustrates how the direct, through-space, 1,4-interaction of the appropriate oxygen lone pairs causes a splitting (Δ_h for the planar, D_{2h}, and Δ_d for the staggered, D_{2d}, conformer) in the energies between the bonding, a_g (or a_1), and the antibonding, b_{1u} (or b_2), lone-pair combinations. To a crude approximation, this interaction should not cause a change in the total energy of the molecule relative to the hypothetical situation corresponding to noninteracting lone pairs, since both the bonding and antibonding combinations are occupied.

In the staggered geometry the direct 1,4-oxygen interaction is reduced to a minimum since the oxygens are staggered and are maximally separated. Consequently, Δ_d is shown to be smaller than Δ_h,[24] with the lone-pair combination of the planar symmetry being more stable than that of the staggered geometry. Mixing occurs between the localized functions of the same symmetry resulting in two occupied molecular orbitals for the a_g (or a_1) manifold, the one of lower energy, $4a_g$ (or $4a_1$), exhibiting considerable N–O nonbonding character while the higher orbital, $6a_g$ (or $6a_1$), is N–O antibonding. Similarly, molecular orbital $5b_{1u}$ (or $5b_2$) is N–O bonding and N–N antibonding, with the charge being centered for the most part on the lone pairs of the oxygen atoms. As found in Tables III and IV, the interactions depicted in Figure 2 are sufficiently strong so that there is a crossing of the oxygen lone-pair contributions resulting in the molecular orbital exhibiting a bonding 1,4 interaction (*i.e.*, $6a_g$ or $6a_1$) being at higher energy than the orbital with an antibonding 1,4 interaction (*i.e.*, $5b_{1u}$ or $5b_2$). Following Hoffmann,[14] this may be interpreted as a "through bond" stabilization of the 1,4-antibonding combination of the oxygen lone pairs by the higher lying N–N σ^* orbital and a destabilization of the 1,4-bonding combination of lone pairs by the lower lying N–N σ orbital.

Since the interaction between the N–N σ^* level and the appropriate symmetry adapted combination of the oxygen lone-pair orbitals has a stabilizing effect, tending to decrease the total energy of the molecule, any change in geometry ought to be favored, other things being equal, if it would increase this interaction by, for instance, decreasing the energy gap between the N–N σ^* function and the lone pairs. In the planar geometry, the higher lying combination of the oxygen lone-pair orbitals exhibits higher energy than the similar combination in the staggered form, thereby promoting incorporation of the virtual N–N σ^* function and thus favoring the planar form. Additional planar-form stabilization results from the fact that the 1,4-lone-pair interaction (stronger in the planar form than in the staggered) is on the whole bonding, due to the removal of part of the antibonding combination *via* elimination into the virtual N–N σ^* orbital.

The electron density in the molecular plane of the $4a_g$, $5b_{1u}$, $6a_g$, and the virtual $6b_{1u}$ molecular orbitals of N_2O_4 is shown in the computer-generated plots of Figure 3. The $4a_g$ orbital at the bottom is clearly N–N bonding and the $6b_{1u}$ N–N antibonding. The $5b_{1u}$ molecular orbital shows effective bonding overlap between the N–N σ^* localized function and the 1,4-antibonding combination of the axially oriented lone pairs. Similarly, for the $6a_g$ molecular orbital, the antibonding interaction of the N–N σ localized function and the 1,4-bonding combination of the lone pairs is evidenced by the nodal surface that separates them.

Obviously, the above analysis of the σ system does not explain the slightly greater stability of the staggered form of B_2F_4 over the planar form. For this molecule, it must be recognized that the fluorine lone pairs are both substantially more compact than the oxygen lone pairs and energetically more stable. The compactness of the orbitals lowers the 1,4-lone-pair interactions, thereby decreasing both Δ_d and Δ_h and the difference between them. Additionally the increased energy gap between the B–B σ^* bond and the 1,4-antibonding combination of the fluorine lone pairs decreases the possibility of deriving conformer stabilization

through preferential delocalization of the fluorine lone-pair orbitals into the B–B σ^* function. Indeed, the lower calculated energy for the staggered with respect to the planar form of the B_2F_4 molecule may be ascribed to the relatively lower electron–electron repulsion in the former. The magnitude of this electrostatic effect may be roughly estimated using the charges derived from the gross Mulliken populations from the *ab initio* calculations in conjunction with a point-charge approximation. Such an energy estimation is found to favor the staggered form by 0.0009 au, a value which is comparable in size and has the same sign as our calculated rotational barrier of 0.0005 au.

Inspection of Tables II through VI provides support for the interpretation presented above. Thus, in Table II, the total A–A σ overlap population is greater for the staggered than for the planar conformer for both the N_2O_4 and B_2F_4 molecules. This difference for either molecule is due in good part to the more negative A–A overlap in the $5b_{1u}$ orbital of the planar form as compared to the $5b_2$ orbital of the staggered. Furthermore, the $5b_{1u}$ orbital exhibits a higher A–Y overlap population and a greater gross atomic population for atom A than does orbital $5b_2$, a finding which is indicative of the greater incorporation of the A–A σ^* function into the molecular orbital of the planar form. Also note the greater energy gap between the $5b_{1u}$ and $5b_2$ orbitals for N_2O_4 as compared to B_2F_4. For both molecules, the highest occupied molecular orbital ($6a_g$ or $6a_1$) exhibits a higher A atomic and a more negative A–Y overlap population in the planar than in the staggered form.

An interesting point is the bonding 1,4 interaction between the oxygens in N_2O_4, which in accord with Epiotis[15] may be interpreted as an attractive 1,4 interaction between the lone pairs due to the "draining off" of some of the 1,4-antibonding character into the virtual N–N σ^* molecular orbital. Table II shows the 1,4-overlap population to be the more strongly bonding by a factor of about 6 in the planar as compared to the staggered conformer of N_2O_4. Some of this increase may be attributed to an increased delocalization of the lone pairs in the planar conformer, but the majority ought simply to be attributed to more effective 1,4 overlapping of the oxygen p orbitals in the planar geometry. Indeed, using overlap of the appropriate Slater-type p orbitals (parallel to the A–A bond) as a criterion, orientation alone is estimated to account for an increase in the 1,4-overlap population by a factor of about 5.

Further analytic exploration was attempted through semiempirical calculations at the extended Hückel level. Except for the data of Table VII, we will not present the numerical results but just the trends indicated. In agreement with the *ab initio* calculations, it was found that the σ contribution to the N–N overlap population was greater in the staggered than in the planar conformation, while the N–O population was greater in the planar. An attempt was made to explore the origin of these effects by eliminating various interactions in the molecule and then recalculating the molecular orbitals and the quantities derived from them. Two different cases were studied. In the first, the 1,4 interaction between the Y atoms was eliminated (thus causing $\Delta_h = \Delta_d = 0$) to give the "drop 1,4" data of Table VII. For both N_2O_4 and B_2F_4, there was an energy shift in favor of the staggered form; *e.g.*, the rotational barrier decreased by a factor of about 5 for N_2O_4. These results support the idea that the 1,4 interactions are primarily responsible for the rotational barrier. A second approach was to delete the previously discussed interactions between the axially oriented p orbitals of the Y atoms and the A atoms. Again shifting of energies occurred favoring the staggered form. The interpretation here is that, although the 1,4 interaction is allowed, donation into the A–A σ^* function is effectively eliminated, thereby negating the stabilization so derived.

Table VII. An Approximate Analysis of the Energies of N_2O_4 and B_2F_4 from Extended Hückel Calculations

	"Full"		"Drop 1,4"	
	Planar D_{2h}	Staggered D_{2d}	Planar D_{2h}	Staggered D_{2d}
		N_2O_4		
E_σ	−319.012	−318.905	−318.813	−318.813
E_π	−66.009		−66.017	
$E_{\pi'}$	−251.755		−251.810	
E_δ	−58.807	−58.807	−58.807	−58.807
$E_\pi + E_{\pi'}$	−317.765	−317.780	−317.828	−317.804
		B_2F_4		
E_σ	−341.020	−341.015	−341.010	−341.010
E_π	−73.402		−73.402	
$E_{\pi'}$	−301.268		−301.269	
E_δ	−72.088	−72.088	−72.088	−72.088
$E_\pi + E_{\pi'}$	−374.670	−374.672	−374.671	−374.673

The foregoing analysis might lead to speculation concerning the relative rotational barriers of B_2F_4 and B_2Cl_4[5] based on the relative ability of fluorine and chlorine to donate into the B–B σ^* bond. The higher acidity of BCl_3 relative to BF_3 has been interpreted in terms of a greater ability of the fluorine lone pairs to back donate into the vacant p orbital of the boron.[25,26]

Semiempirical calculations on BCl_3 and BF_3[27] as well as *ab initio* calculations[28] on B_4Cl_4 and B_4F_4 have shown a lesser lone-pair donation for chlorine than for fluorine. Assuming less lone-pair donation into the B–B σ^* function in B_2Cl_4 than B_2F_4 it follows, by the arguments presented above, that the stability of the planar or D_{2h} conformer of B_2Cl_4 would be lessened relative to that for the D_{2d} staggered. The rotational barrier would depend more completely on the electrostatic interaction of the more diffuse chlorine atoms. However, a second implication of this reasoning is that the B–B bond length in B_2Cl_4 should be shorter than in B_2F_4. This appears to be the case for the solid state ($F_2B–BF_2$ = 1.67 ± 0.04 Å; $Cl_2B–BCl_2$ = 1.75 ± 0.05 Å)[4] but perhaps not in the gaseous ($F_2B–BF_2$ = 1.75 Å).[2a]

Conformer Stabilization by Pi-Type Orbitals.[29] The data of Tables II–VI suggest that the role in conformer stability of the molecular orbitals having lower symmetry than σ will require a particularly detailed explication, since all bonding and antibonding pairs of π- and δ-type orbitals in the valence shell are filled. Furthermore, the differences between the total ($\pi + \pi'$) overlap populations of the planar and staggered conformers are small as compared to the respective σ-type differences, while the δ orbitals show no population changes. In the planar conformer, each π or π' function on one AY_2 unit interacts respectively with a π or π' orbital on the other AY_2 unit; however, in the staggered geometry (see structure 2), the π orbitals of one AY_2 unit interact with the π' orbitals of the other. The consequences of these different modes of interaction are qualitatively explored below.

It is advantageous to discuss the energies of the pi-type interactions between two AY_2 units according to three categories. (1) The formation of bonding and antibonding combinations between the doubly occupied orbitals of the two isolated AY_2 groups. Neglecting for the moment any incorporation of the virtual orbitals into the occupied orbitals thus formed, the net result will be destabilizing. (2) The mixing of the symmetry adapted AY_2 virtual orbitals into the occupied orbitals of the A_2Y_4 molecule, thereby allowing reorganization of the occupied orbitals to provide a stabilization effect. The extent of this mixing will depend on

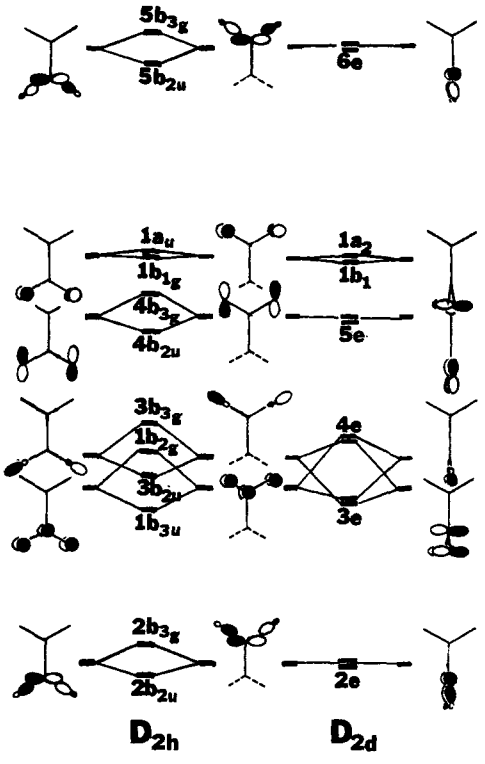

Figure 4. An interaction diagram for the A–A pi-like orbitals of two AY_2 units, as in N_2O_4. On the left, the geometry of interaction is planar, D_{2h}; and, on the right, staggered, D_{2d}. The vertical axis is not proportional to energy. All orbitals except the highest two are occupied.

several factors which are discussed below on the basis that the conformation allowing the greater mixing of the virtual into the occupied orbitals should be the more stable. (3) The repulsive electrostatic interaction between the negatively charged Y atoms. As discussed previously for the σ-type orbitals, this effect will be minimal for the staggered conformation, thereby tending to stabilize it.

In Table VII are presented the results of two sets of extended Hückel calculations. In the first, referred to as "full," a normal calculation of this type was performed, with the orbitals being classified as σ, π, π', or δ types and the appropriate summations of the orbital energies being carried out. In the second set, under the heading "drop 1,4," all 1,4 interactions between the Y atoms were set to zero, thereby providing a qualitative feel for the importance of these contributions.

The "full" extended Hückel results indicate that the pi-type orbitals as a whole are at lower energy in the staggered than in the planar comformation. That the net antibonding 1,4 interactions of the axial lone pairs are responsible for the destabilization of the pi orbitals of the planar conformer may be seen by comparing the "full" to the "drop 1,4" set. In the modified calculation, the cumulative energies of the pi orbitals now favor the D_{2h} form of N_2O_4 instead of the D_{2d} (for B_2F_4 both conformers are of about the same energy).

Having eliminated the 1,4 interactions, the AY_2 fragments still interact at the A atoms where, in the absence of virtual-orbital mixing, the net interaction still ought to be antibonding. Furthermore, we may expect it to be more antibonding in the planar geometry where there are four occupied bonding and antibonding pairs to provide a net destabilizing effect, whereas in the staggered form there are only two strongly interacting pairs, as illustrated by Figure 4. However, the lower energy of the planar pi orbitals in the

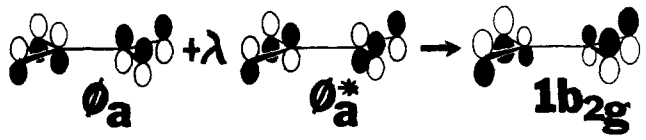

Figure 5. The incorporation of some A–Y antibonding character from virtual orbital ϕ_a^* into the A–A antibonding orbital ϕ_a shifts density away from the A atoms tending to stabilize the molecular orbital. λ is a mixing constant.

"drop 1,4" calculations indicates that there is a factor (obviously of lesser magnitude than the 1,4-lone-pair interaction) which favors the planar form.

Both the extended Hückel and the *ab initio* results indicate that mixing of the AY_2 virtual-orbital combinations into the occupied pi orbitals is greater for the planar geometry. As is exemplified in Figure 5, this mixing leads to strengthening of the A–A interaction in the Y_2A–AY_2 bonding combination and to weakening of it in the antibonding combination. The factors controlling the mixing of the AY_2 virtual orbitals into the occupied orbitals of A_2Y_4 may be given expression by means of perturbation theory.

Consider the mixing of the A–Y bonding and antibonding members of the overall π system of one AY_2 unit with those of the other for the planar geometry, **1**. Neglecting the effect of the overlap term in the normalization process the expressions for the bonding, ϕ, nonbonding, ϕ_n, and virtual antibonding, ϕ^*, π-type functions of an isolated AY_2 unit are

$$\phi^* = c(\mathrm{Np}_\pi) - d(\mathrm{O_1p}_\pi + \mathrm{O_2p}_\pi)/\sqrt{2} \quad (1)$$

$$\phi_n = 1/\sqrt{2}(\mathrm{O_1p}_\pi - \mathrm{O_2p}_\pi) \quad (2)$$

$$\phi = d(\mathrm{Np}_\pi) + c(\mathrm{O_1p}_\pi + \mathrm{O_2p}_\pi)/\sqrt{2} \quad (3)$$

where c and d are constants determined by the variational process.

In the formation of the planar A_2Y_4 molecular orbitals by joining of two AY_2 units, bonding and antibonding combinations are formed from each of these functions, defined in equations 1–3. Thus

$$\phi_a^* = \phi^* - \phi^{*\prime} \quad (4)$$

$$\phi_b^* = \phi^* + \phi^{*\prime} \quad (5)$$

$$\phi_{na} = \phi_n - \phi_n' \quad (6)$$

$$\phi_{nb} = \phi_n + \phi_n' \quad (7)$$

$$\phi_a = \phi - \phi' \quad (8)$$

$$\phi_b = \phi + \phi' \quad (9)$$

where the unprimed quantity represents a combination of atomic orbitals on one AY_2 unit and the primed quantity a combination on the other. The occupied ϕ_{nb} and ϕ_{na} combinations (the symmetry designations of which in the *ab initio* calculations are $1b_{1g}$ and $1a_u$, respectively) do not derive any stabilization from mixing with virtual orbitals and need not concern us further.

We wish to evaluate the extent that ϕ_a^* or ϕ_b^* will mix into the occupied orbital ϕ_a or ϕ_b thereby stabilizing it. Using simple perturbation theory and neglecting all interactions except those arising from bonded atoms we arrive at an approximate expression which measures the mixing of ϕ_a^* into ϕ_a or the mixing of ϕ_b^* into ϕ_b

$$cdH_{A,A'}{}^1/(\epsilon_\phi - \epsilon_{\phi^*}) \quad (10)$$

where $H_{A,A'}{}^1$ represents the element of the perturbation matrix connecting the p_π orbitals on atoms A and A'. (At the Hückel level, this is simply the appropriate element of

the Hückel Hamiltonian matrix which may be evaluated by the Wolfzberg-Helmholtz approximation $H_{A,A'} = H_{A,A'} = \beta_{A,A'}$.)

The important point for our analysis, however, is that the mixing is proportional to the product of the coefficients c and d, which were given in eq 1 and 3 as the coefficients of the p_π orbital on the A atom in the isolated AY_2 fragment. In our crude approximation, the normalization requirement provides that $c^2 + d^2 = 1$ and consequently the product cd will be maximal when $c = d = 2^{-1/2}$. Note that, with these values for c and d, the orbital fragments ϕ and ϕ^* become identical with the bonding and antibonding molecular orbitals of a three-carbon allyl system within the simple Hückel approximation. The result is that the more polar the A–Y π bond the less stabilization will be obtained from incorporation of the virtual orbitals into the occupied molecular orbitals. Accordingly, less stabilization by this means is expected for B_2F_4 than for N_2O_4, for which the A–Y bond is less polar.

The extended Hückel results provide support for the above analysis. Comparing the ratio of the coefficients of the p_π orbitals on the A atom to that on the Y atom for the final ϕ_a and ϕ_b molecular orbitals provides a measure of the importance of the rearrangement of the orbital due to incorporation of virtual-orbital character. For N_2O_4 the ratio is 0.8973 for ϕ_a and 1.1527 for ϕ_b, a difference of 22%. Within the ϕ_b orbital there has been a shift of density toward the bonding nitrogens while in the ϕ_a orbital the shift is away from the now antibonding N–N center. For B_2F_4 the ratios are 0.1945 for ϕ_a and 0.1827 for ϕ_b, a difference of only 6% for the more polar bond.

Returning to Table II it is found that the N–N overlap population in the total π-system set of orbitals of the planar N_2O_4 molecule is substantially less negative than in the respective π' set, a situation which is indicative of a greater incorporation of virtual orbitals in the π set.

After this discussion, we return to the main purpose of comparing the planar and staggered conformers. In N_2O_4, the stabilization obtained by incorporation of virtual orbitals is expected to be greater in the planar than in the staggered form. The reason for this is that the lowest lying virtual pi-type orbital of an AY_2 unit belongs to the π system and is given as ϕ^* in eq 1. As detailed above, the extent to which the virtual ϕ^* orbital is incorporated into the occupied orbital of one of the AY_2 units is proportional to the coefficient of the parallel p orbital (p_π when the conformation is planar, or $p_{\pi'}$ when staggered) on the A atom of the other AY_2 unit. It turns out that the high-lying π' occupied orbitals exhibit little density on the A atom relative to the A atom component of the high-lying occupied π orbital, as may be seen in Table III. Consequently, in the staggered form where a π'-type combines with a π-type orbital fragment, there is little incorporation of the π^* virtual orbitals into the occupied π system as a result of the disparate A-atom participation. This is exemplified by structure **3** which

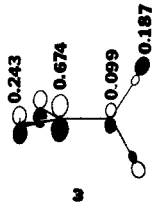

3

shows the Mulliken net atomic populations for one member of the 3e molecular-orbital pair of staggered N_2O_4. The small contribution from the nitrogen on the right, which is part of the π' system, is responsible according to eq 10, for only a small amount of stabilization due to incorporation of the virtual π^* orbital of the system on the left.

The rearrangement of the π orbitals as a result of the mixing-in of the virtual orbital may be examined through the ratio of the net atomic populations for nitrogen to that of oxygen. For planar N_2O_4, molecular orbital $1b_{3u}$, which is N–N π bonding, exhibits a (net N/net O) ratio of 3.027, while, for the antibonding $1b_{2g}$ orbital, the ratio is 2.375. As with the extended Hückel results, the *ab initio* results show that the N–N π-bonding orbital has moved density toward the bonding nitrogens while the antibonding orbital has moved density away from the nitrogens. For the staggered form, the ratio for the π portion of the N–N bonding 3e orbital is 2.773 whereas, for the antibonding 4e orbital, it is 2.488. The greater spread between the ratios for the planar as compared to that for the staggered form is indicative of the greater utilization of the π^* virtual orbital in the planar geometry. Table II shows the total N–N π-overlap population as being less negative for the staggered than for the planar form of N_2O_4. This is simply due to the increased interaction, both bonding and antibonding, that occurs in the staggered form, as explained above.

Summary

The orbitals which are involved in the bonding in N_2O_4 or B_2F_4 are divided up into σ, π, and π' sets. It is argued that the planar geometry observed for N_2O_4 is mainly due to the greater σ-type 1,4 interaction between the oxygen atoms in this geometry, whereas, the reduced rotational barrier of B_2F_4, slightly favoring the staggered form in the *ab initio* calculations, is attributed to the small overlap of the fluorine orbitals and the greater destabilizing electrostatic repulsion that occurs in the planar form.

The factors that make the total π-type orbitals favor either the planar or staggered geometry were explored and the net antibonding interaction between the π orbitals of the AY_2 units was estimated to be smaller for the planar conformation. Of lesser importance, the incorporation of virtual-orbital character (primarily the π^* orbital of an AY_2 unit) is greater in the planar geometry.

Alternative electronic configurations previously suggested for the ground state of N_2O_4 were explored and found to be dissociative.

Acknowledgment. We wish to thank the Air Force Office of Scientific Research, Air Force Systems Command, United States Air Force under AFOSR contract No. AFOSR-72-2265 for partial support of this study. One of us (J.M.H.) wishes to express appreciation for partial support by a Faculty Research Award from the City University of New York. We are also grateful for the donation of substantial computer time at the Central Computer Facility of the City University of New York as well as at the Vanderbilt Computer Center. We are most appreciative of comments by R. D. Harcourt.

References and Notes

(1) (a) D. W. Smith and K. Hedberg, *J. Chem. Phys.*, **25**, 1282 (1956); see also W. G. Fatsley, H. A. Bent, and B. Crawford, Jr., *ibid.*, **31**, 204 (1959); P. Groth, *Nature (London)*, **198**, 1081 (1963); B. Cartwright and J. H. Robertson, *Chem. Commun.*, **3**, 82 (1966); (b) B. W. McClelland, G. Gundersen, and K. Hedberg, *J. Chem. Phys.*, **56**, 4541 (1972).

(2) (a) L. A. Nimon, K. S. Seshadri, R. C. Taylor, and D. White, *J. Chem. Phys.*, **53**, 2416 (1970); J. V. Patton and K. Hedberg, Abstracts of Second Austin Symposium on Gas Phase Molecular Structure, The University of Texas at Austin, Feb. 26–27, 1968, p M5; J. N. Gayles and J. Self, *J. Chem. Phys.*, **40**, 3530 (1964); A. Finch, J. Hyams, and D. Steele, *Spectrochim. Acta*, **21**, 1423 (1965); for B_2Cl_4: K. Hedberg and R.

Ryan, *J. Chem. Phys.*, **41**, 2214 (1964); R. Ryan and K. Hedberg, *ibid.*, **50**, 4986 (1969); (b) J. R. Durig, J. W. Thompson, J. D. Witt, and J. D. Odom, *ibid.*, **58**, 5339 (1973).
(3) R. G. Snyder and I. C. Hisatsune, *J. Mol. Spectrosc.*, **1**, 139 (1957).
(4) L. Trefonas and W. N. Lipscomb, *J. Chem. Phys.*, **28**, 54 (1958); for B_2Cl_4: M. Atoji, P. J. Wheatley, and W. N. Lipscomb, *ibid.*, **27**, 196 (1957).
(5) K. Hedberg, *Trans. Amer. Crystallogr. Assoc.*, **2**, 79 (1966); R. R. Ryan and K. Hedberg, *J. Chem. Phys.*, **50**, 4986 (1969).
(6) C. A. Coulson and J. Duchesne, *Bull. Cl. Sci., Acad. Roy. Belg.*, **43**, 552 (1957).
(7) (a) R. D. Brown and R. D. Harcourt, *Proc. Chem. Soc., London*, 216 (1961); (b) R. D. Brown and R. D. Harcourt, *Aust. J. Chem.*, **18**, 1885 (1965).
(8) J. Serre, *Mol. Phys.*, **4**, 269 (1961); R. LeGoff and J. Serre, *Theor. Chim. Acta*, **1**, 66 (1962).
(9) (a) M. Green and J. W. Linnett, *Trans. Faraday Soc.*, **57**, 1, 10 (1961); (b) L. Burnelle, P. Beaudouin, and L. J. Schaad, *J. Phys. Chem.*, **71**, 2240 (1967); (c) T. F. Redmond and B. B. Wayland, *ibid.*, **72**, 3038 (1968); (d) R. D. Brown and R. D. Harcourt, *Aust. J. Chem.*, **16**, 737 (1963); **18**, 1118 (1965); (e) R. D. Harcourt, *Theor. Chim. Acta*, **2**, 437 (1964); **4**, 202 (1966); **6**, 131 (1966); *Int. J. Quantum Chem.*, **4**, 173 (1970); **18**, 115 (1965); R. D. Harcourt, *J. Mol. Struct.*, **9**, 221 (1971); **8**, 11 (1971); (f) G. Leroy, M. Van Meerssche, and G. Germain, *J. Chim. Phys. Physicochem. Biol.*, **60**, 1282 (1963); (g) M. Green and J. W. Linnett, *Trans. Faraday Soc.*, **57**, 10 (1961); (h) L. Pauling, "The Nature of the Chemical Bond," 2nd ed, Cornell University Press, Ithaca, N.Y., 1960, p 349; (i) V. K. Kelkar, K. C. Bhalla, and P. G. Khubchandan, *J. Mol. Struct.*, **9**, 383 (1971).
(10) E. G. Moore, *Theor. Chim. Acta*, **7**, 144 (1967); R. D. Brown and R. D. Harcourt, *Aust. J. Chem.*, **16**, 737 (1963); A. H. Cowley, W. D. White, and M. C. Damasco, *J. Amer. Chem. Soc.*, **91**, 1922 (1969).
(11) M. Green and J. W. Linnett, *J. Chem. Soc.*, 4959 (1960); H. Kata, K. Yamaguichi, T. Yonezawa, and K. Fukui, *Bull. Chem. Soc. Jap.*, **38**, 2144 (1965). See also C. J. S. Schutte, *Spectrum*, 6, 263 (1968).
(12) M. F. Guest and I. H. Hillier, *J. Chem. Soc., Faraday Trans. 2*, **70**, 398 (1974).
(13) An exception is ref 9c.
(14) W.-D. Stohrer and R. Hoffmann, *J. Amer. Chem. Soc.*, **94**, 779 (1972); R. Hoffmann, *Accounts Chem. Res.*, **4**, 1 (1971).
(15) N. D. Epiotis, *J. Amer. Chem. Soc.*, **95**, 3087 (1973); N. D. Epiotis and W. Cherry, *J. Chem. Soc., Chem. Commun.*, 278 (1973); N. D. Epiotis, D. Bjorkquist, and S. Sarkanen, *J. Amer. Chem. Soc.*, **95**, 7558 (1973).
(16) Our choice of axes is such that for the D_{2h} geometry vectors parallel to the A–A axis, perpendicular to the A–A axis but in the molecular plane, and perpendicular to the plane transform as B_{1u}, B_{2u}, and B_{3u}, respectively.
(17) The Gaussian exponents in the 52/52 calculations were: (N) s 553.3, 84.91, 19.62, 5.421, 0.4201 and p 2.333, 0.4148; (O) s 736.6, 112.9, 26.04, 7.212, 0.5764 and p 2.333, 0.4148; (B) s 258.4, 40.19, 9.342, 2.579, 0.1900 and p 0.9285, 0.1681; (F) s 948.5, 144.9, 33.46, 9.261, 0.7528 and p 4.190, 0.7106.
(18) The Gaussian exponents in the 73/73 calculations were: (N) s 1619., 248.7, 57.75, 16.36, 5.081, 0.7797, 0.2350 and p 6.273, 12.82, 0.2974; (O) s 2200., 332.2, 76.93, 21.74, 6.773, 1.103, 0.3342 and p 8.356, 1.719, 0.3814; (B) s 738.0, 114.4, 26.79, 7.723, 2.426, 0.3538, 0.1134 and p 2.713, 0.5336, 0.1251; (F) s 2723., 416.4, 97.73, 27.87, 8.712, 1.396, 0.4209 and p 10.53, 2.168, 0.4785.
(19) R. Hoffmann, *J. Chem. Phys.*, **39**, 1397 (1963).
(20) Slater exponents: (N) 1.95; (O) 2.275; (B) 1.300; (F) 2.424. H_{ii}: (N) 2s −26.0 eV and 2p −13.4; (O) 2s −32.3 and 2p −14.8; (B) 2s −15.2 and 2p −8.5; (F) 2s −40.0 and 2p −18.1.
(21) G. B. B. M. Sutherland, *Proc. Roy. Soc., London*, **141**, 342 (1933).
(22) G. Hertzberg, "Infra-Red and Raman Spectra," Van Nostrand, New York, N.Y., 1945, p 184.
(23) Although molecular orbitals $1b_{1g}$ and $1a_u$ exhibit nodal-plane structures of δ symmetry with respect to the A–A bond axis, we call these electronic configurations $\Pi 1$ and $\Pi 2$ because the net bonding for them is provided by π orbitals.
(24) We have attempted to assign numerical values to Δ_h and Δ_d for N_2O_4 by means of the extended Hückel approximation employing oxygen 2p Slater orbitals oriented parallel to the N–N axis. Within this approximation $\Delta_h = 0.42$ eV and $\Delta_d = 0.17$ eV. We believe that while the Δ_h/Δ_d ratio is proably nearly right these values are too low. As the interatomic separation becomes large single ζ Slater orbitals demonstrate overlap which is increasingly too small relative to that of atomic orbitals expressed in terms of larger basis sets. Compare the single ζ Slater overlaps with those obtained by using the oxygen 2p SCF eigenfunctions expressed in our three p-type Gaussians: with $r = 1.16$ Å, overlap $S_{2p_\sigma,2p_\sigma}$, 1STO = 0.319 (3GTO = 0.274); $r = 2.09$, 1STO = 0.063 (3GTO = 0.193); $r = 3.02$, 1STO = 0.005 (3GTO = 0.028).
(25) H. C. Longuet-Higgins, *Quart. Rev., Chem. Soc.*, **11**, 121 (1957).
(26) W. N. Lipscomb, "Boron Hydrides," W. A. Benjamin, New York, N.Y., 1963.
(27) M. Lappert, M. Litzow, J. Pedley, P. Riley, and A. Tweedale, *J. Chem. Soc. A*, 3105 (1968).
(28) J. H. Hall, Jr., and W. N. Lipscomb, *Inorg. Chem.*, **13**, 710 (1974).
(29) The term "pi" refers collectively to π and π' type orbitals.

Synthesis and Structural Characterization of a New Cyanomanganate(III) Complex, Heptapotassium μ-Oxo-bis[pentacyanomanganate(III)]cyanide

Ronald F. Ziolo, Richard H. Stanford, George R. Rossman, and Harry B. Gray*

Contribution No. 4896 from the Arthur Amos Noyes Laboratory of Chemical Physics, California Institute of Technology, Pasadena, California 91125. *Received May 31, 1974*

Abstract: The final product resulting from the reaction of $KMnO_4$ and KCN in saturated aqueous solution is a gold-brown compound $K_7[(CN)_5MnOMn(CN)_5]CN$, as established by a single-crystal X-ray diffraction study. Full-matrix least-squares refinement included anisotropic temperature parameters for all atoms and converged with a final R index (on F) of 0.091. The structure contains the oxo bridged $[Mn_2O(CN)_{10}]^{6-}$ ion, which has $2/m$ crystallographic symmetry with the bridging oxygen atom lying at a center of symmetry. The ion exists in an eclipsed rotomeric configuration. The Mn–O distance is relatively short, 1.723 (4) Å. Crystallographically independent potassium ions are coordinated to the nitrogen ends of cyanide groups in trigonal prismatic, octahedral, and square antiprismatic geometries. Crystal data are as follows: orthorhombic; space group *Ibam*; $a = 12.397$ (8), $b = 12.772$ (8), $c = 14.618$ (7) Å (temperature 23°); $Z = 4$; $d_{obsd} = 1.98$, $d_{calcd} = 1.97$ g/cm^3. The synthesis, isolation, and physical characteristics of $K_7[Mn_2O(CN)_{10}]CN$ are reported along with spectral and magnetic data. The principal features in the infrared spectrum are cyanide stretching bands centered around 2090 cm^{-1}. The optical absorption spectrum in a KBr pellet consists of a primary band at 370 nm with a prominent shoulder at 410 nm and a weak shoulder at approximately 610 nm. The gold-brown crystals are strongly pleochroic, the crystals being colorless when the E vector is parallel to the long needle axis. This characteristic serves as a convenient means of identification for this substance. At room temperature $K_7[Mn_2O(CN)_{10}]CN$ is diamagnetic.

In 1930 Yakimach[1] reported that the action of KCN on $KMnO_4$ in saturated aqueous solution led to a red crystalline substance of composition $K_4[Mn(CN)_8]$, which decomposed in water giving HCN and MnO_2. It was suggested, assuming this composition, that the salt was a crystal aggregate of $K_2Mn(CN)_6$ and 2KCN.[2] Goldenberg,[3] in an attempt to prepare this double cyanide of tetravalent manganese, noted that when using Yakimach's preparation, *i.e.*, saturated aqueous $KMnO_4$ (6.7%) and a solution containing 80 g of KCN to 100 g H_2O, a bulky precipitate of